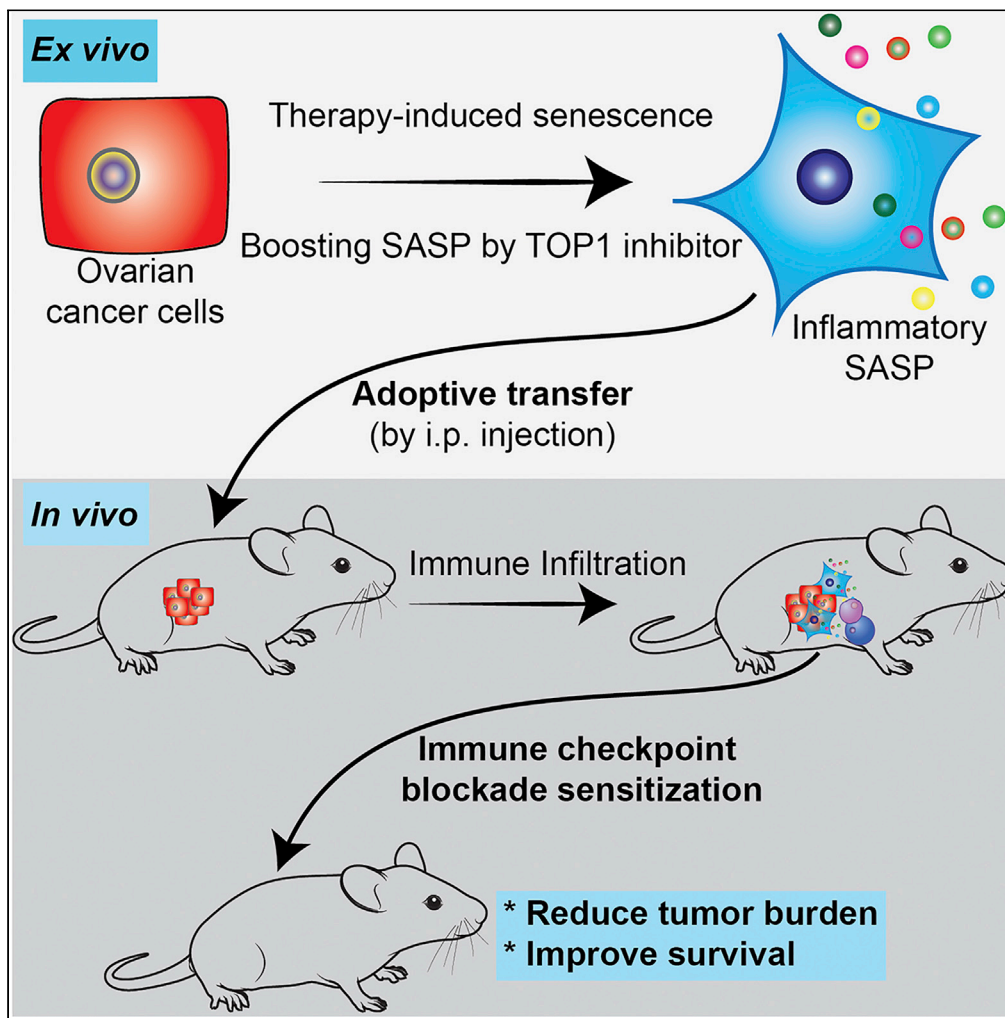


Article

Sensitization of ovarian tumor to immune checkpoint blockade by boosting senescence-associated secretory phenotype



Xue Hao, Bo Zhao, Wei Zhou, Heng Liu, Takeshi Fukumoto, Dmitry Gabrilovich, Rugang Zhang

rzhang@wistar.org

**HIGHLIGHTS**

TOP1 inhibitors boost SASP in platinum-induced senescent ovarian cancer cells

Enhancement of SASP by TOP1 inhibitor is mediated by the cGAS pathway

Adoptive transfer of SASP-boosted senescent cells sensitizes ovarian tumor to ICB

Sensitization to ICB correlates with an increase in immune infiltration

Hao et al., iScience 24, 102016  
January 22, 2021 © 2020 The Author(s).  
<https://doi.org/10.1016/j.isci.2020.102016>



## Article

## Sensitization of ovarian tumor to immune checkpoint blockade by boosting senescence-associated secretory phenotype

Xue Hao,<sup>1,3</sup> Bo Zhao,<sup>1,3</sup> Wei Zhou,<sup>1</sup> Heng Liu,<sup>1</sup> Takeshi Fukumoto,<sup>1</sup> Dmitry Gabrilovich,<sup>1,2</sup> and Rugang Zhang<sup>1,4,\*</sup>

## SUMMARY

**Therapy-induced senescence-associated secretory phenotype (SASP) correlates with overcoming resistance to immune checkpoint blockade (ICB). Intrinsic resistance to ICB is a major clinical challenge. For example, ovarian cancer is largely resistant to ICB. Here we show that adoptive transfer of SASP-boosted ex vivo therapy-induced senescent cells sensitizes ovarian tumor to ICB. Topoisomerase 1 (TOP1) inhibitors such as irinotecan enhance cisplatin-induced SASP, which depends on the TOP1 cleavage complex-regulated cGAS pathway. Significantly, intraperitoneal transfer of cisplatin-induced, SASP-boosted senescent cells with irinotecan sensitizes ovarian tumor to anti-PD-1 antibody and improves the survival of tumor-bearing mice in an immunocompetent, syngeneic model. This correlates with the infiltration of transferred senescent cells in the established orthotopic tumors and an increase in the infiltration of activated CD8<sup>+</sup> T cells and dendritic cells in the tumor bed. Our findings indicate that adoptive transfer of SASP-boosted therapy-induced senescent cells represents a potential therapeutic strategy to sensitize tumors to ICB.**

## INTRODUCTION

Cellular senescence is a bona fide tumor suppression mechanism that can be induced by a number of stresses including chemotherapeutics such as cisplatin (Herranz and Gil, 2018). Therapy-induced senescence is tumor suppressive by triggering a stable cell growth arrest (Herranz and Gil, 2018). Senescent cells also have non-cell autonomous activities exemplified by secretion of inflammatory cytokines and chemokines, which is termed the senescence-associated secretory phenotype (SASP) (Coppe et al., 2008). The pattern recognition cGAS-STING pathway plays an important role in regulating senescence and associated SASP (Dou et al., 2017; Gluck et al., 2017; Takahashi et al., 2018; Yang et al., 2017). The topoisomerase 1 cleavage complex (TOP1cc) is necessary for cGAS-mediated regulation of SASP during senescence (Zhao et al., 2020). TOP1 is responsible for relaxing higher order topological DNA structures during DNA replication and gene transcription (Pommier et al., 2016). TOP1 forms the stable protein-DNA TOP1 cleavage complex (TOP1cc) through its enzymatic activity and TOP1 becomes covalently bound to the catalytically generated DNA strand break (Pommier et al., 2016). Clinically applicable TOP1 inhibitors such as irinotecan induce TOP1cc by trapping TOP1 on DNA (Pommier et al., 2016).

Immune checkpoint blockades (ICBs) such as monoclonal antibodies targeting the PD-1/PD-L1 axis have demonstrated striking clinical benefit in several cancer types (Darvin et al., 2018). However, despite this important advance, the majority of cancers show unacceptably low response rates to ICB (O'Donnell et al., 2017). Therefore, new therapeutic strategies are urgently needed to expand the utility of ICBs through sensitizing ICB resistant tumors.

Ovarian cancer remains the most lethal gynecological malignancy in the developed world. Tumor-infiltrating lymphocytes positively correlate with ovarian cancer patient survival, which is recognized as a predictive biomarker for immunotherapy and chemotherapy responses (Zhang et al., 2003). Notably, CD8<sup>+</sup> T cells are important antitumor effectors in ovarian cancer (Sato et al., 2005). However, objective response rates to ICB in ovarian cancer range from 5.9 to 15% (Wang et al., 2019). Therefore, sensitizing ICB resistant ovarian cancer to ICB remains an unmet clinical need.

<sup>1</sup>Immunology, Metastasis and Microenvironment Program, The Wistar Institute, Philadelphia, PA 19104, USA

<sup>2</sup>AstraZeneca, Oncology R&D, Gaithersburg, MD 20878, USA

<sup>3</sup>These authors contributed equally

<sup>4</sup>Lead contact

\*Correspondence: rzhang@wistar.org

<https://doi.org/10.1016/j.isci.2020.102016>



cGAS is essential for SASP (Dou et al., 2017; Gluck et al., 2017; Takahashi et al., 2018; Yang et al., 2017) and for the antitumor effect of ICB such as anti-PD-L1 antibody (Xiang et al., 2017). In addition, induction of inflammatory SASP by a CDK4/6 inhibitor correlates with overcoming ICB resistance in melanoma in a CD8<sup>+</sup> T cells dependent manner (Jerby-Arnon et al., 2018; Wagner and Gil, 2020). Likewise, a combination of MEK and CDK4/6 inhibitors in pancreatic ductal adenocarcinoma produces a SASP that stimulates the accumulation of CD8<sup>+</sup> T cells into otherwise immunologically “cold” tumors and sensitizes tumors to PD-1 checkpoint blockade (Ruscetti et al., 2020). However, therapeutic strategies that leverage SASP of senescent cells to sensitize resistant tumors to ICB remain to be fully explored. For example, whether adoptive transfer of SASP-boosted *ex vivo* therapy-induced senescent cells can be used as a cell therapy to sensitize resistant tumors to ICB has never been investigated. Here we show that adoptive transfer of SASP-boosted, cisplatin-induced senescent ovarian cancer cells using a clinically applicable TOP1 inhibitor sensitizes ovarian tumor to anti-PD-1 treatment.

## RESULTS

### Isolation of SASP-boosted, therapy-induced senescent ovarian cancer cells

To isolate senescent cells for adoptive transfer, we treated UPK10 mouse ovarian cancer cells with cisplatin to induce senescence as evidenced by induction of markers of senescence including senescence-associated  $\beta$ -galactosidase (SA- $\beta$ -Gal) activity, p16 and  $\gamma$ H2AX (Figures 1A–1C). This was accompanied by a decrease in cell proliferation marker cyclin A (Figure 1C). UPK10 cells were isolated from mouse ovarian tumors developed from conditional activation of *Kras* and inactivation of *Tp53* that fully recapitulated the immune microenvironment of human ovarian cancers (Scarlett et al., 2012). In addition, platinum-based chemotherapies such as cisplatin are standard of care for ovarian cancer (Lheureux et al., 2019). We chose 10  $\mu$ M cisplatin based on optimal induction of SASP factors such as *IL1 $\beta$* , *IL8*, and *CXCL10* in a dose-titration study (Figure S1A). Since TOP1 inhibitors enhance SASP without affecting senescence-associated growth arrest (Zhao et al., 2020), we combined cisplatin and a clinically applicable TOP1 inhibitor irinotecan (Pommier et al., 2016). The dose of irinotecan was determined based on optimal induction of SASP factors such as *IL1 $\beta$* , *IL8*, and *CXCL10* as well as TOP1cc in a dose-titration study (Figures S1B and S1C). Notably, the percentage of senescent cells induced by cisplatin with or without irinotecan was comparable as determined by a fluorescence-based marker of senescence, SPiDER SA- $\beta$ -Gal activity (Figure 1D). Interestingly, irinotecan alone also induced SA- $\beta$ -Gal activity, which is consistent with the notion that activation of TOP1cc-regulated cGAS pathway induces senescence and SASP (Yang et al., 2017). Next, we sorted senescent cells induced by a combination of cisplatin and irinotecan using flow cytometry based on expression of fluorescence SPiDER SA- $\beta$ -Gal activity and larger sizes of senescent cells (Figures 1E and 1F). Notably, flow cytometry sorting did not significantly stress the senescent cells to increase cell death (Figure S1D). Validating our senescent cells sorting strategy, cell proliferation markers such as BrdU incorporation was negative in re-cultured, sorted senescent cells compared with non-senescent cells even after three weeks of culture (Figure 1G). Similar results were also obtained in ID8 mouse ovarian cancer cells (Figures S1E–S1K), indicating that this is not a cell line specific effect. Finally, to examine the growth potential of the sorted senescent cells *in vivo*, we orthotopically transplanted the sorted senescent cells into mouse bursa that covers the mouse ovary to mimic the *in vivo* tumor microenvironment. Notably, sorted control non-senescent cells formed tumors that reached ethical limit in one month. In contrast, sorted senescent cells that were orthotopically transplanted in parallel failed to form visible tumors in two and half months (Figure 1F). Together, we conclude that it is feasible to sort out growth-arrested, therapy-induced senescent cells *in vitro*.

### TOP1 inhibitor irinotecan boosts SASP through the cGAS pathway

We next sought to characterize the sorted senescent cells from the different treatment groups. Compared with cisplatin-induced senescent cells, TOP1cc levels were increased by irinotecan addition (Figure 2A). Interestingly, TOP1cc levels were notably higher in the sorted non-senescent cells treated with irinotecan or a combination compared with vehicle control treated non-senescent cells (Figure 2A). However, these cells are not senescent as evidenced by expression of cell proliferation markers such as cyclin A (Figure 2A). This suggests that TOP1cc alone is not sufficient to induce senescence. We next examined changes in expression of SASP factors by quantitative reverse transcription polymerase chain reaction (qRT-PCR) in the sorted non-senescent and senescent cells from the various treatment groups. Indeed, irinotecan significantly increased the expression of SASP factors induced by cisplatin at the mRNA levels (Figure 2B), which correlated with an increase in SASP regulators such as phospho-p65 NF- $\kappa$ B and phospho-p38 MAPK (Figure 2A) (Herranz and Gil, 2018). Validating our sorting approach, the sorted non-senescent cells did not show overt increase in the expression of SASP factors (Figure 2B). Similar findings were also made in ID8 mouse ovarian cancer cells (Figures S2A and S2B). We further validated the increase in the secretion of

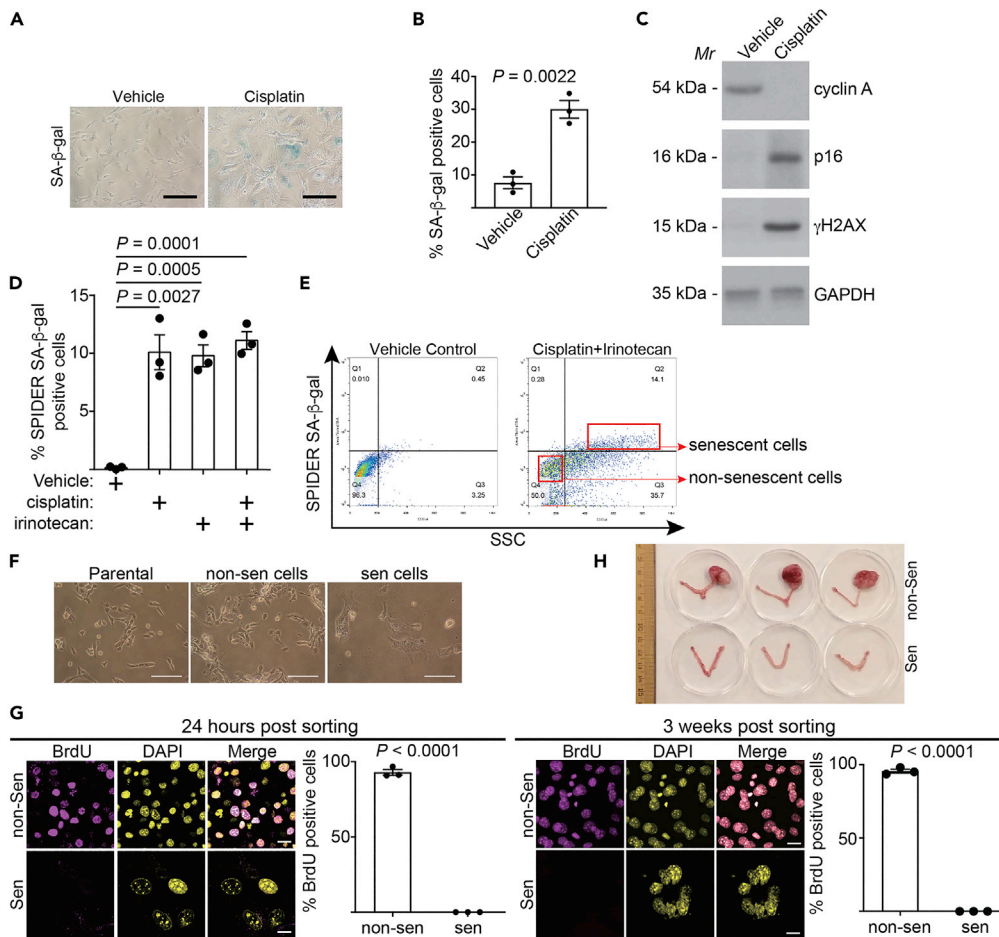


**Figure 1. Isolation of SASP-boosted therapy-induced senescent cells**

(A–C) UPK10 cells were treated with 10  $\mu$ M cisplatin for three days. After three days of release, cells were stained for SA- $\beta$ -gal activity (A) and percentage of SA- $\beta$ -gal positive cells were quantified (B). Expression of the indicated proteins was also examined by immunoblot in the indicated cells (C).

(D) UPK10 cells were treated with 10  $\mu$ M cisplatin, 10  $\mu$ M irinotecan, or a combination for three days and released for three days. SA- $\beta$ -gal positive cells were quantified using SPIDER SA- $\beta$ -gal assay by flow cytometry.

(E and F) UPK10 cells were treated with a combination of 10  $\mu$ M cisplatin and 10  $\mu$ M irinotecan for three days and released for three days. Senescent and non-senescent cells were sorted using gating strategies indicated in (E). Phase contrast images of sorted non-senescent and senescent UPK10 cells after replating were shown (F).

(G) Sorted senescent and non-senescent cells from cisplatin and irinotecan treated UPK10 cells at the indicated time points post sorting (24 hrs and 3 weeks) were labeled with BrdU for 24 hrs and BrdU incorporation was examined by immunofluorescence staining and quantified.

(H) 1  $\times$  10<sup>6</sup> sorted senescent and non-senescent cisplatin and irinotecan treated UPK10 cells (n=3 mice per group) were orthotopically transplanted into mouse bursa that covers mouse ovary. Shown are images of ovaries with tumor formed by non-senescent cells in one month and those without evidence of tumor formation by sorted senescent cells after two and half months.

Data represent mean  $\pm$  SEM of 3 biologically independent experiments. Scale bar = 100  $\mu$ m in 1A and 1F, and = 20  $\mu$ m in 1G. *p* values were calculated using a two-tailed *t* test. See also Figure S1.

SASP factors induced by irinotecan and cisplatin combination using an antibody array (Figures 2C and 2D). As a control, DMAXX, an STING agonist in mouse cells (Conlon et al., 2013), is sufficient to increase the expression and secretion of SASP factors, albeit at a significantly lower levels compared with those in the senescent cells sorted from cisplatin and irinotecan combination treatment (Figures 2B–2D, S2C, and S2D). Together, we conclude that TOP1 inhibitor irinotecan boosts SASP in the senescent cells induced by cisplatin.

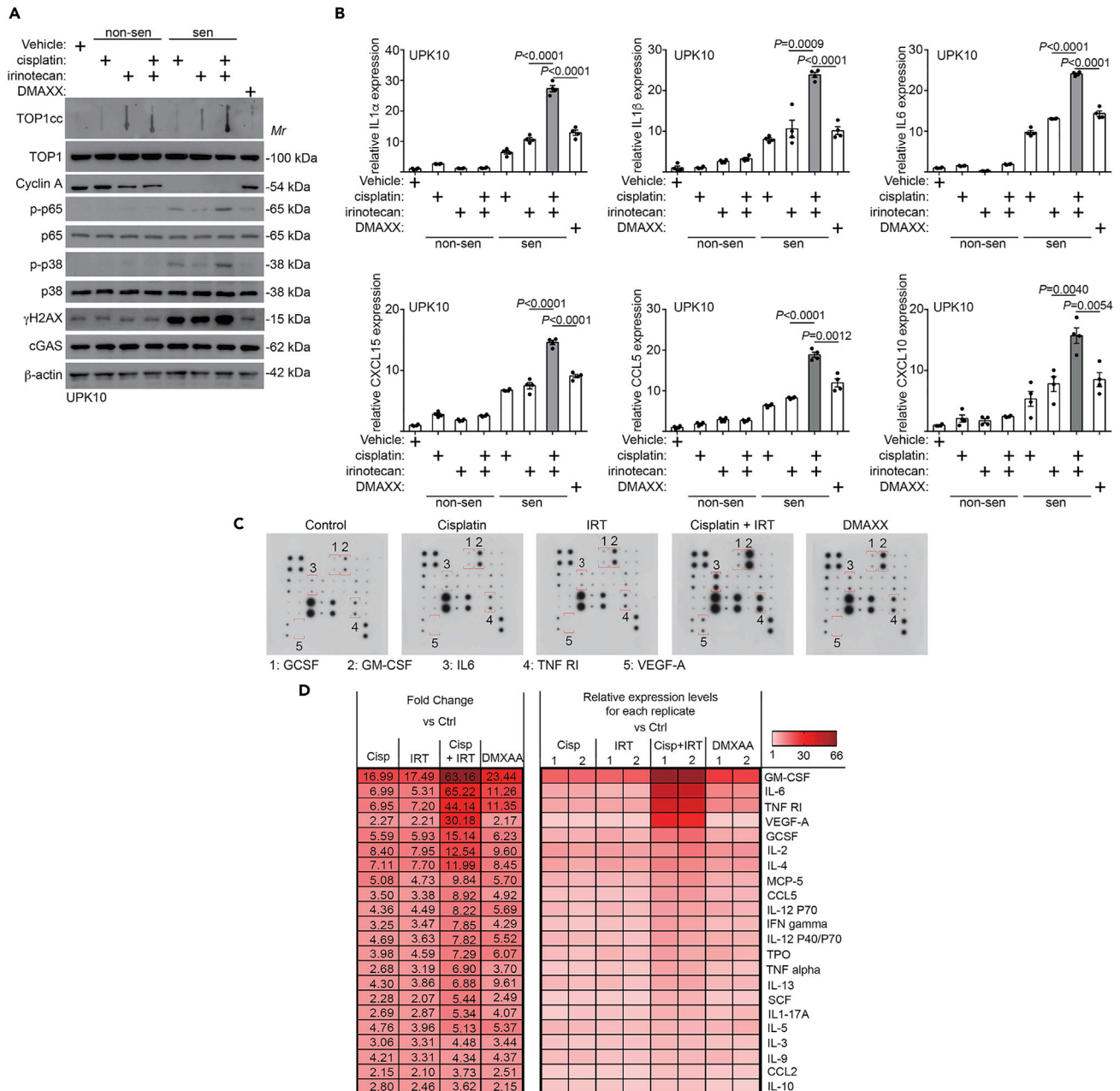


**Figure 2. TOP1 inhibitor irinotecan boosts SASP expression.**

(A and B) UPK10 cells were treated with 10 $\mu$ M cisplatin, 10 $\mu$ M irinotecan, a combination or 10  $\mu$ M DMXAA for three days and released for three days. Expression of TOP1cc, TOP1, cyclin A, phosphor-p65, total p65, phosphor-p38 MAPK, total p38 MAPK,  $\gamma$ H2AX, cGAS, and a loading control  $\beta$ -actin was examined by immunoblot in the sorted non-senescent and senescent cells from the indicated treatment groups (A). Expression of the indicated SASP factors in sorted senescent and non-senescent UPK10 cells from the indicated treatment groups was determined by qRT-PCR (B). (n=3 biologically independent experiments).

(C and D) Secretion of SASP factors under the indicated conditions was determined using an antibody array (C). Examples of changes in the secreted SASP factors were highlighted. The heatmap indicates the fold change (FC) in comparison with the control (Ctrl) UPK10 cells. Relative expression levels per replicate and average fold change differences are shown (D).

Data represent mean  $\pm$  SEM. p values were calculated using a two-tailed t test. See also Figure S2 and Table S1.

We next sought to determine whether the observed enhancement of SASP by irinotecan is TOP1 and cGAS dependent. Toward this goal, we knocked down TOP1 or cGAS using two independent shRNAs to limit potential off-target effects (Figures 3A and 3B). Consistently, TOP1 knockdown decreased TOP1cc levels

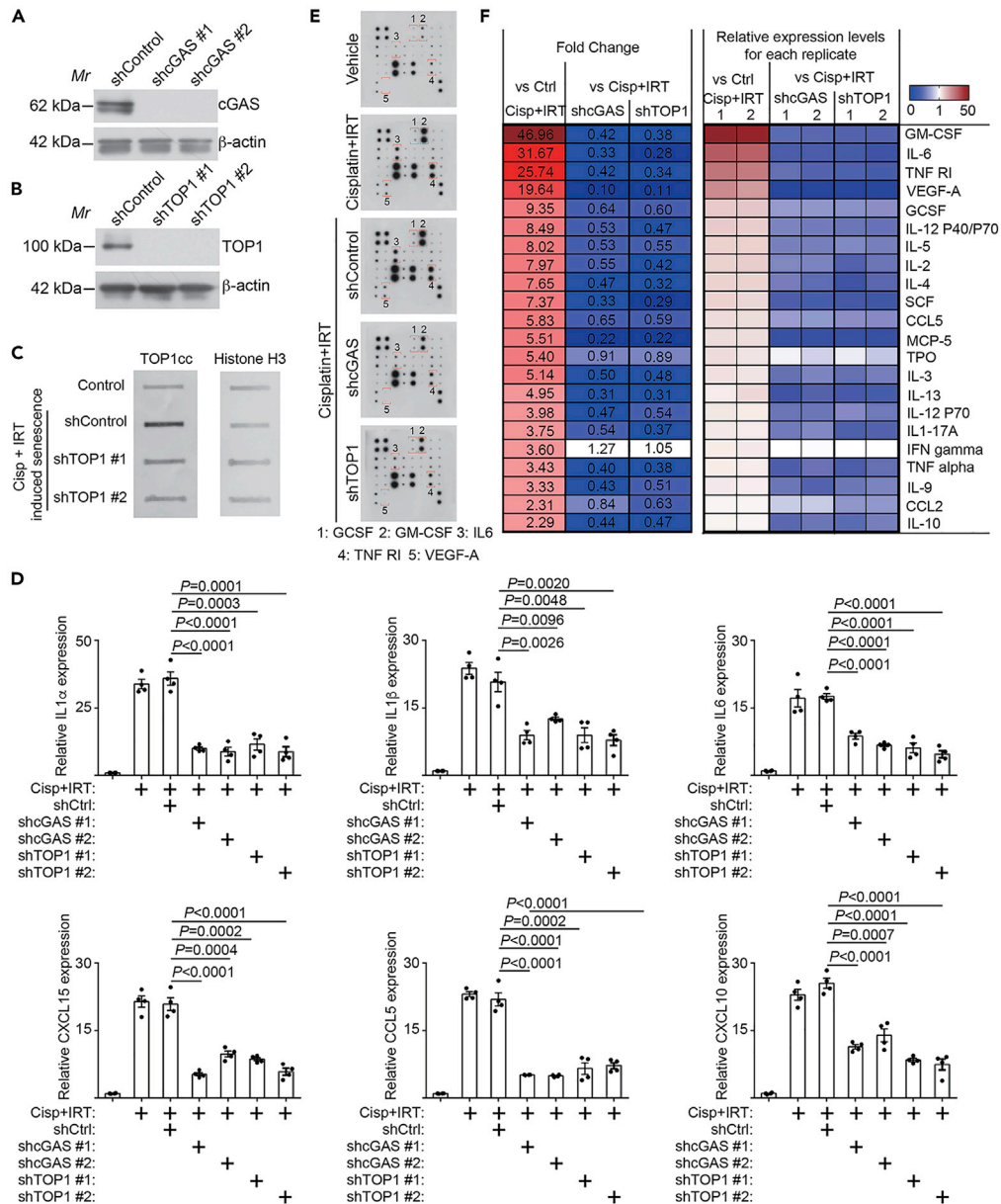


**Figure 3. TOP1 inhibitor irinotecan boosts SASP through TOP1cc-regulated cGAS pathway**

(A) Expression of TOP1 and a loading control  $\beta$ -actin in UPK10 cells expressing the indicated shTOP1s or a shControl was determined by immunoblot.

(B) Expression of cGAS and a loading control  $\beta$ -actin in UPK10 cells expressing the indicated shcGASs or a shControl was determined by immunoblot.

(C) Expression of TOP1cc in UPK10 cells expressing the indicated shTOP1s or a shControl was determined by slot blot. Expression of histone H3 was used as a control.

(D) UPK10 cells were treated with  $10\mu\text{M}$  cisplatin,  $10\mu\text{M}$  irinotecan, or a combination for three days and released for three days. Expression of the indicated SASP factors in the sorted non-senescent and senescent cells was determined by qRT-PCR ( $n = 3$  biologically independent experiments).

(E and F) Secretion of SASP factors under the indicated conditions was determined by an antibody array (E). Examples of changes in the secreted SASP factors were highlighted. The heatmap indicates the fold change (FC) in comparison with the control (Ctrl) or senescent UPK10 cells sorted from cisplatin and irinotecan combination treatment (Cisp + IRT). Relative expression levels per replicate and average fold change differences are shown (F). Data represent mean  $\pm$  SEM of  $p$  values were calculated using a two-tailed t test. See also [Figure S3](#).

induced by irinotecan and cisplatin combination (Figure 3C). Indeed, knockdown of either TOP1 or cGAS significantly suppressed the expression of SASP genes as determined by qRT-PCR (Figure 3D). Consistently, secretion of SASP factors was also significantly decreased by knockdown of either cGAS or TOP1 in the sorted senescent cells induced by cisplatin and irinotecan combination (Figures 3E and 3F). Together, these findings support the notion that the observed enhancement of SASP by irinotecan in cisplatin-induced senescent cells was mediated by TOP1cc-regulated cGAS pathway.

### Transfer of SASP-boosted senescent cells sensitizes ovarian tumor to anti-PD-1 antibody

Given the critical role played by cGAS in mediating ICB (Xiang et al., 2017) and the evidence that induction of inflammatory SASP correlates with sensitization of resistant melanomas to ICB (Jerby-Arnon et al., 2018), we sought to explore the possibility of adoptive transfer of SASP-boosted senescent cells as a potential cell therapy to sensitize tumors to ICB. Toward this goal, we established a syngeneic, immunocompetent mouse ovarian tumor model using UPK10 cells (Scarlett et al., 2012). We orthotopically transplanted UPK10 into the mouse bursa and allowed the tumor to establish for two weeks (Figure 4A). We transplanted sorted control non-senescent or senescent UPK10 cells induced *ex vivo* by cisplatin, irinotecan or a combination by *i.p.* injection on day 15 and 22 and followed with anti-PD-1 antibody treatment on day 16, 19, 23, and 26 (Figure 4A). To differentiate the pre-established tumors formed by GFP-positive UPK10 cells from those of *i.p.* injected UPK10 cells, we labeled the subsequently injected sorted control non-senescent and senescent cells with mCherry that are GFP and mCherry double positive (Figure S4A). Notably, both non-senescent and senescent mCherry positive cells infiltrated the pre-established GFP-positive orthotopic tumors formed by GFP-positive UPK10 cells (Figure 4B). This result suggests that the adoptively transferred, SASP-boosted senescent ovarian cancer cells are capable of infiltrating the pre-existing tumor sites. Notably, anti-PD-1 antibody was not effective against the pre-established UPK10 tumors compared with IgG controls (Figures 4C–4E). Interestingly, senescent cells sorted from the cisplatin or irinotecan treatment alone did not significantly reduce tumor burden in response to anti-PD-1 antibody treatment (Figures 4C–4E). However, the injection of sorted SASP-boosted senescent cells induced by a combination of cisplatin and irinotecan significantly reduced the tumor burden as indicated by a reduction in tumor weight (Figures 4C–4E, group 6). Consistently, the survival of the tumor-bearing mice in this group was significantly improved (Figure 4F). Notably, the injection of sorted non-senescent control cells did not increase tumor growth (Figures 4C–4E). This might be caused by partial effects of anti-PD-1 antibody treatment in this group or a masking effect caused by the growth of the pre-established tumors. Consistent with previous reports that SASP-accompanied sensitization of ICB is mediated by CD8<sup>+</sup> T cell (Jerby-Arnon et al., 2018), we observed an increase in infiltrated activated CD69<sup>+</sup>/CD8<sup>+</sup> T cells in the tumor bed in group 6 (Figures 4G and S4B). In addition, we observed an increase in CD11b<sup>+</sup> dendritic cells in group 6 compared with other groups (Figure 4G). There was an increase in infiltration of activated CD69<sup>+</sup>/CD4<sup>+</sup> T cells in group 6 compared with group 4, but not group 5 (Figure S4C). Notably, transfer of DMXAA *ex vivo* treated cells did not affect the response to anti-PD-1 and failed to reduce tumor burden or improve the survival of tumor-bearing mice (Figures 4C–4F). Consistently, neither CD69<sup>+</sup>/CD8<sup>+</sup> T cells nor CD11b<sup>+</sup> dendritic cells were significantly affected by the transfer of DMXAA *ex vivo* treated cells (Figure 4G). Notably, no overt toxicity associated with adoptive transfer of SASP-boosted, cisplatin-induced senescent ovarian cancer cells was observed. For example, the body weight of tumor-bearing mice was not significantly reduced compared with other treatment groups (Figure S4D). Together we conclude that adoptive transfer of SASP-boosted cisplatin-induced senescent ovarian cancer cells using TOP1 inhibitor irinotecan sensitizes ovarian tumors to ICBs.

## DISCUSSION

Despite the fact that SASP-promoting cGAS is required for response to ICB (Xiang et al., 2017) and therapy-induced SASP correlates with overcoming resistance to ICBs (Jerby-Arnon et al., 2018; Ruscetti et al., 2020), therapeutic approaches that leverage SASP of senescent cells to sensitize tumors to ICB have not been reported. Here we show that adoptive transfer of SASP-boosted, cisplatin-induced senescent cells using clinically applicable TOP1 inhibitor irinotecan sensitizes ovarian tumor to ICB. An advantage of this approach is that the treatment occurs *ex vivo*, which will limit the potential systematic toxicity caused by direct treatment with these small molecules *in vivo*. Consistent with our findings, TOP1 inhibitors increase the sensitivity of patient-derived melanoma cell lines to T-cell-mediated cytotoxicity (Haggerty et al., 2011; McKenzie et al., 2018).

Notably, the observed sensitization correlates with infiltration of senescent cells into the tumor bed. Indeed, previous studies show that intravenously or subcutaneously injected ovarian cancer cells

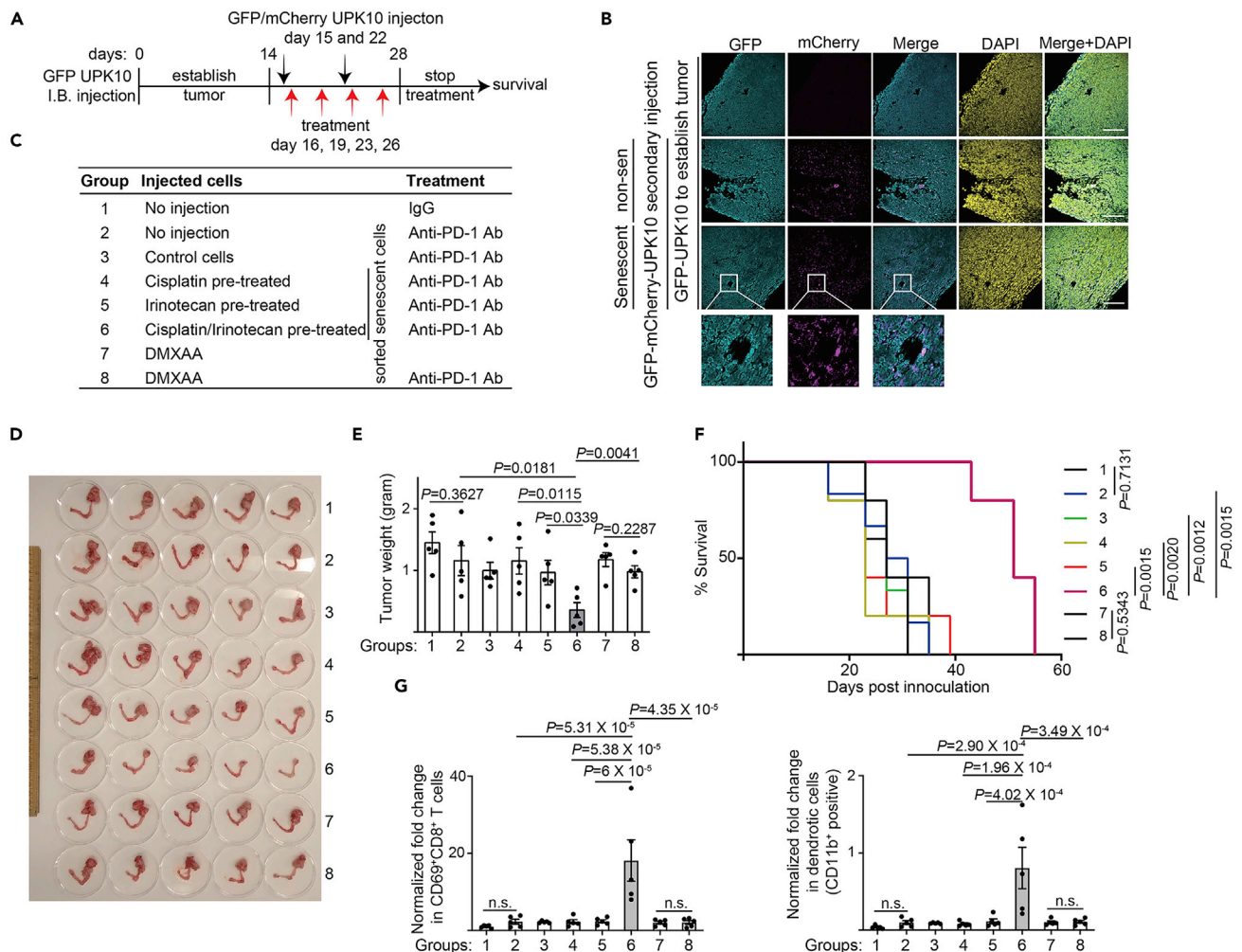


**Figure 4. Adoptive transfer of SASP-boosted therapy-induced senescent cells sensitizes ovarian tumor to anti-PD-1 treatment**

(A) Schematics of experimental design. GFP-expressing UPK10 cells were orthotopically transplanted into the mouse bursa for two weeks to allow for tumor formation. The indicated control or sorted senescent UPK10 cells *ex vivo* induced by cisplatin, irinotecan or a combination of cisplatin and irinotecan were i.p. injected on day 15 and 22 and followed with anti-PD-1 antibody treatment on day 16, 19, 23 and 26. In addition, transfer of DMXAA *ex vivo* treated UPK10 cells were included as a control. Note that sorted non-senescent cells were used as control cells.

(B) At the end of two weeks of treatment, immunofluorescent staining revealed infiltration of injected non-senescent and senescent UPK10 cells (GFP and mCherry double positive) into the pre-established orthotopic tumors (only GFP-positive).

(C) Outline of experimental groups into which mice were randomized. Please note that control cells are sorted non-senescent cells.

(D and E) At the end of two weeks of treatment, reproductive tracts with tumors from the indicated treatment groups were dissected (D) and tumor weights were measured as a surrogate for tumor burden (E). (n = 5 biologically independent mice per group).

(F) After stopping the treatment, the mice from the indicated groups were followed for survival. Shown are the Kaplan–Meier survival curves of mice from the indicated treatment groups (n = 5 biologically independent mice per group).

(G) Fold changes in percentage of CD69<sup>+</sup>/CD8<sup>+</sup> T cells in CD8<sup>+</sup> T cell population and CD11b<sup>+</sup> dendritic cells in dendritic cell population (normalized by tumor weight) were determined in tumors dissected from the indicated treatment groups (n = 5 biologically independent mice per group).

Data represent mean ± SEM. Scale bar = 200 μm in 4B. P-values were calculated using two-tailed t test in 4E, log-rank (Mantel–Cox) test in 4F, and multiple test in 4G. n.s.: not significant. See also Figure S4.

metastasize to ovary (Bai et al., 2019). This raised the possibility that transfer of SASP-boosted senescent cells may convert “cold” into “hot” tumors through infiltration of senescent cells into tumor bed and associated secretion of inflammatory SASP factors. However, we cannot exclude the possibility that the transferred senescent cells may localize to other areas. In addition, further studies are warranted to elucidate what SASP factors mediate the observed antitumor response and what cells are being impacted to regulate therapy response. Further, this approach in combination with subsequent ICB treatment may allow for

targeting and eradicating residual tumor nodules to prevent relapse, a major challenge in clinical management of ovarian cancer.

Although cisplatin-induced senescent cells are positive for SASP, their adoptive transfer was not sufficient to sensitize tumors to ICB. This supports the notion that levels of SASP dictate the outcome of adoptively transferred senescent cells. Consistently, STING agonist alone stimulated the expression of the SASP factors to a level that is comparable to those observed in cisplatin-induced senescent cells. However, this is not sufficient to sensitize tumors to ICB. Notably, UPK10 cells were isolated from mouse ovarian tumors developed from conditional activation of *Kras* and inactivation of *Tp53* (Scarlett et al., 2012). In contrast, ID8 is wild-type for both *Kras* and *Tp53*. Given the fact that irinotecan boosted SASP induced by cisplatin in both UPK10 and ID8 cells, these findings suggest that the observed effects are independent of *Kras* or *Tp53* status.

There is evidence that transplantation of *in vitro* generated senescent cells such as adipose-derived mesenchymal stem cells induces physical dysfunction in mice (Xu et al., 2018), which cautions approaches involving transfer of senescent cells. However, the adoptively transferred senescent cells in the present study may be subsequently eliminated by ICB treatment once they infiltrated the pre-existing tumors and potentially altered the tumor microenvironment. Thus, transplanted senescent cells may only be present transiently without potential long-term side effects. Likewise, although we did not observe tumor formation *in vivo* by the orthotopically transplanted senescent cells, it is possible that the transplanted senescent cells may eventually grow *in vivo* after an extended period of times. Our future studies will formally examine these possibilities. In summary, our findings support that adoptive transfer of SASP-boosted, therapy-induced senescent cells represents a potential cell therapy strategy to sensitize tumors to ICB.

### Limitations of the study

A limitation of our study is that we only tested this approach in an ovarian cancer syngeneic mouse model due to availability of suitable models. For example, ID8 syngeneic mouse model is sensitive to ICB, which prevented us from testing this approach (data not shown). Further studies are warranted to test this strategy using additional immunocompetent models such as humanized patient-derived xenograft and in other cancer types with low response rates to ICB.

### Resource availability

#### Lead contact

Further information and requests for resources and reagents should be directed to and will be fulfilled by the lead contact, Rugang Zhang (rzhang@wistar.org).

#### Material availability

This study did not generate new unique reagents.

#### Data and code availability

This study did not generate/analyze datasets/code. The raw data supporting the current study are available from the lead contact upon request. All software is commercially available.

## METHODS

All methods can be found in the accompanying [Transparent Methods supplemental file](#).

## SUPPLEMENTAL INFORMATION

Supplemental information can be found online at <https://doi.org/10.1016/j.isci.2020.102016>.

## ACKNOWLEDGMENTS

We thank Mr. Sean Hua for technical assistance. This work was supported by US National Institutes of Health grants (R01CA160331, R01CA163377, R01CA202919, R01CA239128, and R01CA243142 to R.Z., P01AG031862 to R.Z., and P50CA228991 to R.Z.), US Department of Defense (OC180109 and OC190181 to R.Z.), The Honorable Tina Brozman Foundation for Ovarian Cancer Research and The Tina Brozman Ovarian Cancer Research Consortium 2.0 (to R.Z.) and Ovarian Cancer Research Alliance (Collaborative

Research Development Grant #596552 to R.Z.). Support of Core Facilities was provided by Cancer Center Support Grant (CCSG) CA010815 to The Wistar Institute.

## AUTHOR CONTRIBUTIONS

X.H., B.Z., W.Z., H.L. and T.F. performed the experiments and analyzed data. X.H., B.Z. and R.Z. designed the experiments. D.G. contributed to study design. B.Z., X.H. and R.Z. wrote the manuscript. R.Z. conceived and supervised the study.

## DECLARATION OF INTERESTS

B.Z. and R.Z. are co-inventors of a patent application covering the use of transfer senescent cells to sensitize tumors to ICB. D.G. is an employee of AstraZeneca. All other authors have no competing interests.

Received: August 5, 2020

Revised: December 2, 2020

Accepted: December 28, 2020

Published: January 22, 2021

## REFERENCES

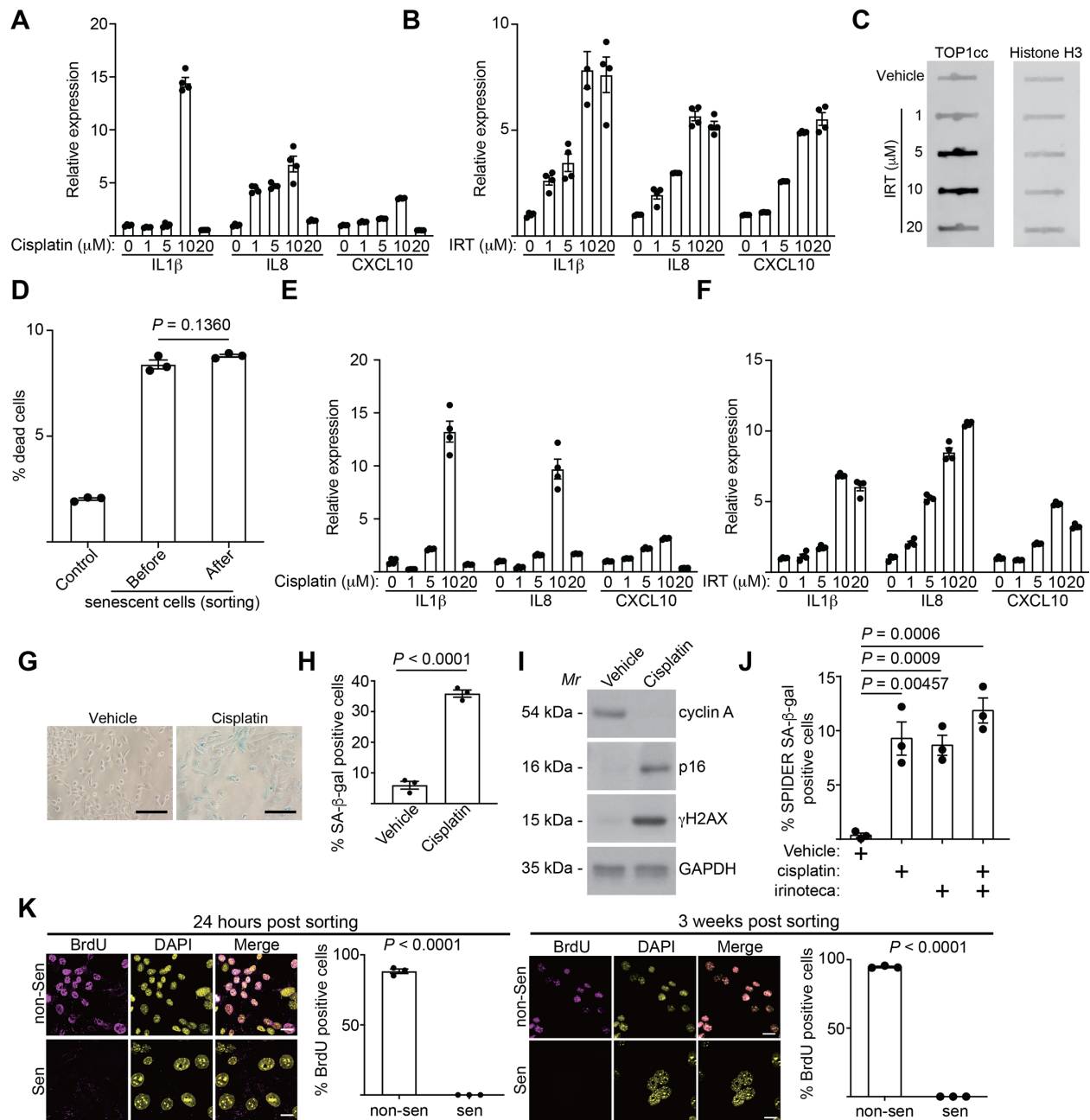
- Bai, S., Zhu, W., Coffman, L., Vlad, A., Schwartz, L.E., Elishaev, E., Drapkin, R., and Buckanovich, R.J. (2019). CD105 is expressed in ovarian cancer precursor lesions and is required for metastasis to the ovary. *Cancers (Basel)* 11, 1710.
- Conlon, J., Burdette, D.L., Sharma, S., Bhat, N., Thompson, M., Jiang, Z., Rathinam, V.A., Monks, B., Jin, T., Xiao, T.S., et al. (2013). Mouse, but not human STING, binds and signals in response to the vascular disrupting agent 5,6-dimethylxanthenone-4-acetic acid. *J. Immunol.* 190, 5216–5225.
- Coppe, J.P., Patil, C.K., Rodier, F., Sun, Y., Munoz, D.P., Goldstein, J., Nelson, P.S., Desprez, P.Y., and Campisi, J. (2008). Senescence-associated secretory phenotypes reveal cell-nonautonomous functions of oncogenic RAS and the p53 tumor suppressor. *PLoS Biol.* 6, 2853–2868.
- Darvin, P., Toor, S.M., Sasidharan Nair, V., and Elkord, E. (2018). Immune checkpoint inhibitors: recent progress and potential biomarkers. *Exp. Mol. Med.* 50, 1–11.
- Dou, Z., Ghosh, K., Vizioli, M.G., Zhu, J., Sen, P., Wangenstein, K.J., Simithy, J., Lan, Y., Lin, Y., Zhou, Z., et al. (2017). Cytoplasmic chromatin triggers inflammation in senescence and cancer. *Nature* 550, 402–406.
- Gluck, S., Guey, B., Gulen, M.F., Wolter, K., Kang, T.W., Schmacke, N.A., Bridgeman, A., Rehwinkel, J., Zender, L., and Ablasser, A. (2017). Innate immune sensing of cytosolic chromatin fragments through cGAS promotes senescence. *Nat. Cell Biol.* 19, 1061–1070.
- Haggerty, T.J., Dunn, I.S., Rose, L.B., Newton, E.E., Martin, S., Riley, J.L., and Kurnick, J.T. (2011). Topoisomerase inhibitors modulate expression of melanocytic antigens and enhance T cell recognition of tumor cells. *Cancer Immunol. Immunother.* 60, 133–144.
- Herranz, N., and Gil, J. (2018). Mechanisms and functions of cellular senescence. *J. Clin. Invest.* 128, 1238–1246.
- Jerby-Arnon, L., Shah, P., Cuoco, M.S., Rodman, C., Su, M.J., Melms, J.C., Leeson, R., Kanodia, A., Mei, S., Lin, J.R., et al. (2018). A cancer cell program promotes T cell exclusion and resistance to checkpoint blockade. *Cell* 175, 984–997 e924.
- Lheureux, S., Braunstein, M., and Oza, A.M. (2019). Epithelial ovarian cancer: evolution of management in the era of precision medicine. *CA Cancer J. Clin.* 69, 280–304.
- McKenzie, J.A., Mbongu, R.M., Malu, S., Zhang, M., Ashkin, E., Devi, S., Williams, L., Tieu, T., Peng, W., Pradeep, S., et al. (2018). The effect of topoisomerase I inhibitors on the efficacy of T-cell-based cancer immunotherapy. *J. Natl. Cancer Inst.* 110, 777–786.
- O'Donnell, J.S., Long, G.V., Scolyer, R.A., Teng, M.W., and Smyth, M.J. (2017). Resistance to PD1/PDL1 checkpoint inhibition. *Cancer Treat. Rev.* 52, 71–81.
- Pommier, Y., Sun, Y., Huang, S.N., and Nitiss, J.L. (2016). Roles of eukaryotic topoisomerases in transcription, replication and genomic stability. *Nat. Rev. Mol. Cell Biol.* 17, 703–721.
- Ruscetti, M., Morris, J.P., Mezzadra, R., Russell, J., Leibold, J., Romesser, P.B., Simon, J., Kulick, A., Ho, Y.J., Fennell, M., et al. (2020). Senescence-induced vascular remodeling creates therapeutic vulnerabilities in pancreatic cancer. *Cell* 181, 424–441 e421.
- Sato, E., Olson, S.H., Ahn, J., Bundy, B., Nishikawa, H., Qian, F., Jungbluth, A.A., Frosina, D., Gnjjatic, S., Ambrosone, C., et al. (2005). Intraepithelial CD8+ tumor-infiltrating lymphocytes and a high CD8+/regulatory T cell ratio are associated with favorable prognosis in ovarian cancer. *Proc. Natl. Acad. Sci. U S A* 102, 18538–18543.
- Scarlett, U.K., Rutkowski, M.R., Rauwerdink, A.M., Fields, J., Escovar-Fadul, X., Baird, J., Cubillos-Ruiz, J.R., Jacobs, A.C., Gonzalez, J.L., Weaver, J., et al. (2012). Ovarian cancer progression is controlled by phenotypic changes in dendritic cells. *J. Exp. Med.* 209, 495–506.
- Takahashi, A., Loo, T.M., Okada, R., Kamachi, F., Watanabe, Y., Wakita, M., Watanabe, S., Kawamoto, S., Miyata, K., Barber, G.N., et al. (2018). Downregulation of cytoplasmic DNases is implicated in cytoplasmic DNA accumulation and SASP in senescent cells. *Nat. Commun.* 9, 1249.
- Wagner, V., and Gil, J. (2020). Senescence as a therapeutically relevant response to CDK4/6 inhibitors. *Oncogene* 39, 5165–5176.
- Wang, W., Liu, J.R., and Zou, W. (2019). Immunotherapy in ovarian cancer. *Surg. Oncol. Clin. N. Am.* 28, 447–464.
- Xiang, Y., Laurent, B., Hsu, C.H., Nachtergaele, S., Lu, Z., Sheng, W., Xu, C., Chen, H., Ouyang, J., Wang, S., et al. (2017). RNA m(6A) methylation regulates the ultraviolet-induced DNA damage response. *Nature* 543, 573–576.
- Xu, M., Pirtskhalava, T., Farr, J.N., Weigand, B.M., Palmer, A.K., Weivoda, M.M., Inman, C.L., Ogrodnik, M.B., Hachfeld, C.M., Fraser, D.G., et al. (2018). Senolytics improve physical function and increase lifespan in old age. *Nat. Med.* 24, 1246–1256.
- Yang, H., Wang, H., Ren, J., Chen, Q., and Chen, Z.J. (2017). cGAS is essential for cellular senescence. *Proc. Natl. Acad. Sci. U S A* 114, E4612–E4620.
- Zhang, L., Conejo-Garcia, J.R., Katsaros, D., Gimotty, P.A., Massobrio, M., Regnani, G., Makrigiannakis, A., Gray, H., Schlienger, K., Liebman, M.N., et al. (2003). Intratumoral T cells, recurrence, and survival in epithelial ovarian cancer. *N. Engl. J. Med.* 348, 203–213.
- Zhao, B., Liu, P., Fukumoto, T., Nacarelli, T., Fatkhutdinov, N., Wu, S., Lin, J., Aird, K.M., Tang, H.Y., Liu, Q., et al. (2020). Topoisomerase 1 cleavage complex enables pattern recognition and inflammation during senescence. *Nat. Commun.* 11, 908.

iScience, Volume 24

## **Supplemental Information**

### **Sensitization of ovarian tumor to immune checkpoint blockade by boosting senescence-associated secretory phenotype**

**Xue Hao, Bo Zhao, Wei Zhou, Heng Liu, Takeshi Fukumoto, Dmitry  
Gabrilovich, and Rugang Zhang**



**Supplemental Figure 1: Isolation of SASP-boostered therapy-induced senescent cells, related to Figure 1.**

(A-C) UPK10 cells were treated with the indicated concentration of cisplatin (A) or irinotecan (B-C) for three days. After three days of release, expression of the indicated SASP factors was examined by qRT-PCR (A-B). Level of TOP1cc in the irinotecan-treated cells was examined by slot blot (C). (n=4 biologically independent experiments).

(D) Percentage of dead cells in senescent UPK10 cells induced by a combination of 10  $\mu\text{M}$  cisplatin and 10  $\mu\text{M}$  irinotecan before and after flow cytometry sorting. (n=3 biologically independent experiments).

**(E-F)** ID8 cells were treated with the indicated concentration of cisplatin (**E**) or irinotecan (**F**) for three days. After three days of release, expression of the indicated SASP factor was examined by qRT-PCR. (n=4 biologically independent experiments).

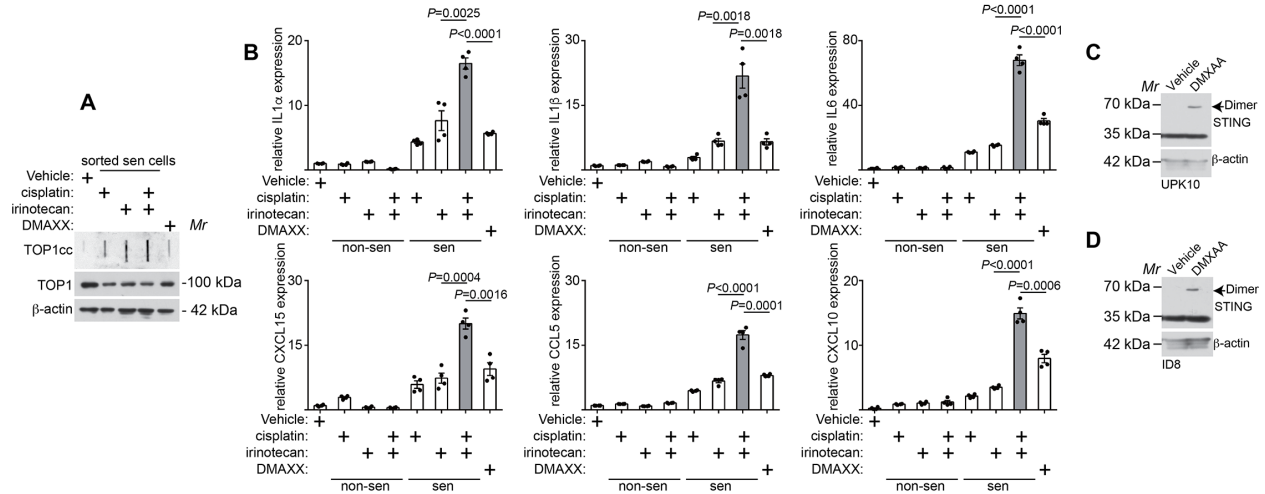
**(G-I)** ID8 cells were treated with 10 $\mu$ M cisplatin for three days and released for three days. SA- $\beta$ -gal activity was examined (**G**) and quantified (**H**). Expression of the indicated proteins were examined by immunoblot in the indicated cells (**I**).

**(J)** ID8 cells were treated with 10 $\mu$ M cisplatin, 10 $\mu$ M irinotecan or a combination for three days and released for three days. SA- $\beta$ -gal positive cells were quantified using SPiDER SA- $\beta$ -gal assay by flow cytometry.

**(K)** Sorted senescent and non-senescent cells from cisplatin and irinotecan treated ID8 cells at the indicated time points post sorting (24 hrs or 3 weeks) were labeled with BrdU for 24 hrs and BrdU incorporation was examined by immunofluorescence staining and quantified.

(n=3 biologically independent experiments).

Data represent mean  $\pm$  SEM. Scale bar = 100  $\mu$ m in S1G and 20  $\mu$ m in S1K. *P* values were calculated using a two-tailed *t*-test.



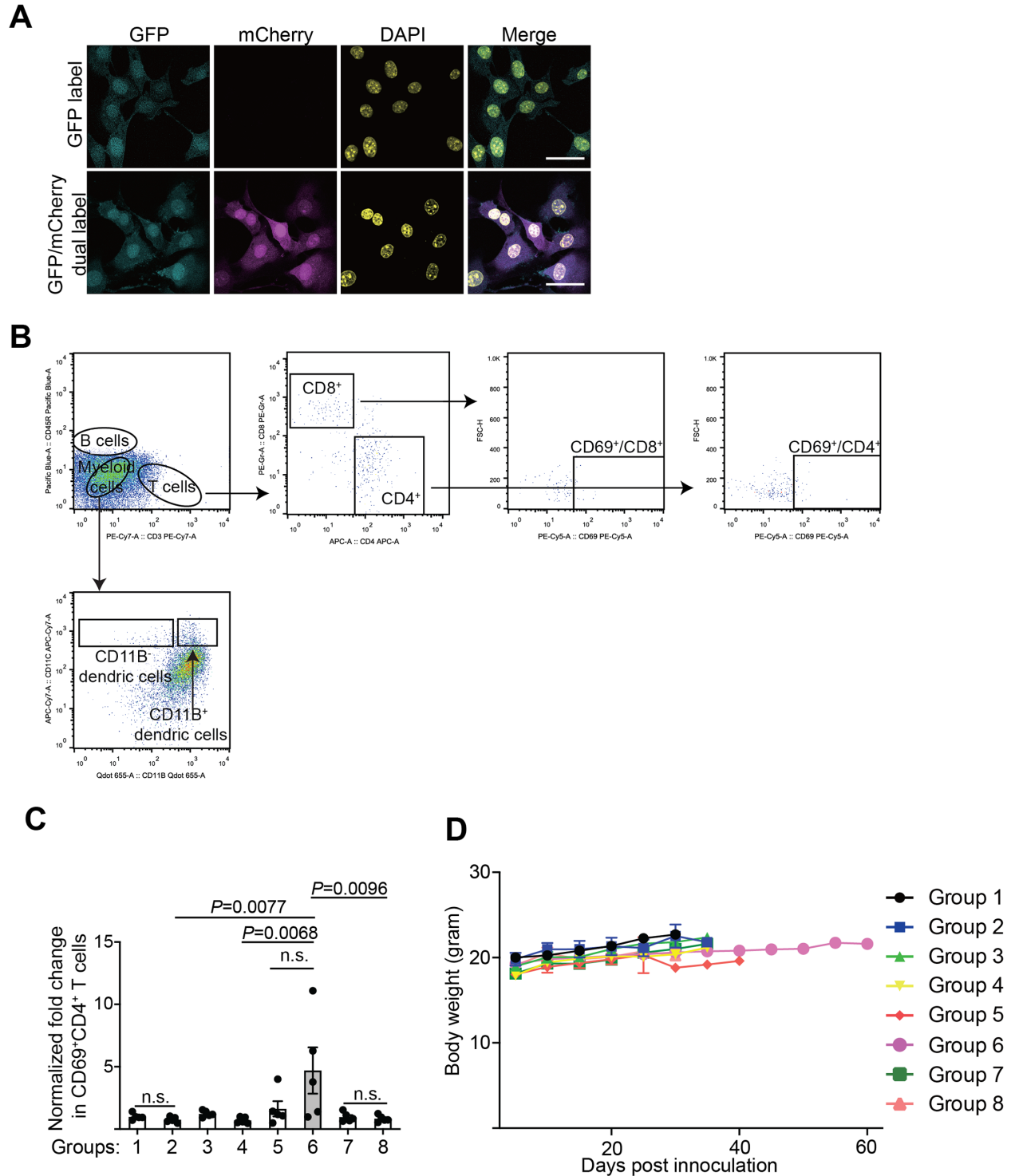
**Supplemental Figure 2: TOP1 inhibitor irinotecan boosts SASP expression in cisplatin-induced ID8 senescent cells, related to Figure 2.**

(A-B) ID8 cells were treated with 10 $\mu$ M cisplatin, 10 $\mu$ M irinotecan, a combination, or 10  $\mu$ M DMXAA for three days and released for three days. Expression of TOP1cc, TOP1 and a loading control  $\beta$ -actin examined by immunoblot in the indicated cells (A). Expression of the indicated SASP factors in sorted senescent and non-senescent ID8 cells from the indicated treatment was determined by qRT-PCR (n=3 biologically independent experiments) (B).

(C-D) STING dimerization induced by DMXAA treatment was determined by immunoblot in UPK10 (C) and ID8 (D) cells.

Data represent mean  $\pm$  SEM. *P* values were calculated using a two-tailed *t*-test.





**Supplemental Figure 4: Adoptive transfer of SASP-boosted senescent cells does not display overt toxicity, related to Figure 4.**

**(A)** Confirmation of GFP and mCherry expression in UPK10 cells used for generating pre-established tumors and adoptive transfer. GFP positive cells were used to generate orthotopic tumors, and GFP and mCherry double positive cells were used for senescence induction and subsequent transfer.

**(B)** The gating strategy used in the present study.

**(C)** Fold changes in percentage of CD69<sup>+</sup>/CD4<sup>+</sup> T cells in CD4<sup>+</sup> T cell population (normalized by tumor weight) were determined in tumors dissected from the indicated treatment groups (n = 5 biologically independent mice per group).

**(D)** Body weight of mice from the indicated treatment groups during the entire experimental period (n = 5 biologically independent mice per group).

Data represent mean  $\pm$  SEM. Scale bar = 20  $\mu$ m in S4A. *P*-values were calculated using multiple *t* test. n.s.: not significant

**Supplemental Table 1: The oligonucleotides used for quantitative RT-PCR, related to Figure 2.**

<b>Name</b>	<b>Sequence</b>	<b>Application</b>
Mouse <i>IL1<math>\alpha</math></i> forward	5'-CCAGAAGAAAATGAGGTCCG-3'	RT-qPCR
Mouse <i>IL1<math>\alpha</math></i> reverse	5'-AGCGCTCAAGGAGAAGACC-3'	RT-qPCR
Mouse <i>IL1<math>\beta</math></i> forward	5'-TGTGCAAGTGTCTGAAGCAGC-3'	RT-qPCR
Mouse <i>IL1<math>\beta</math></i> reverse	5'-TGGAAGCAGCCCTTCATCTT-3'	RT-qPCR
Mouse <i>IL6</i> forward	5'-GCTACCAAAGTGGATATAATCAGGA-3'	RT-qPCR
Mouse <i>IL6</i> reverse	5'-CCAGGTAGCTATGGTACTCCAGAA-3'	RT-qPCR
Mouse <i>CXCL15</i> forward	5'-AGAGGCTTTTCATGCTCAACA-3'	RT-qPCR
Mouse <i>CXCL15</i> reverse	5'-CCATGGGTGAAGGCTACTGT-3'	RT-qPCR
Mouse <i>CCL5</i> forward	5'-CCACTTCTTCTCTGGGTTGG-3'	RT-qPCR
Mouse <i>CCL5</i> reverse	5'-GTGCCCACGTCAAGGAGTAT-3'	RT-qPCR
Mouse <i>CXCL10</i> forward	5'-TCAGCACCATGAACCCAAG-3'	RT-qPCR
Mouse <i>CXCL10</i> reverse	5'-CTATGGCCCTCATTCTCACTG-3'	RT-qPCR
Mouse <i>B2M</i> forward	5'-AGTTAAGCATGCCAGTATGGCCGA-3'	RT-qPCR
Mouse <i>B2M</i> reverse	5'-ACATTGCTATTTCTTTCTGCGTGC-3'	RT-qPCR

## Transparent Methods

KEY RESOURCES TABLES

CONTACT FOR REAGENT AND RESOURCES SHARING

EXPERIMENTAL MODEL AND SUBJECT DETAILS

Cell lines

Mice

METHODS AND DETAILS

Lentivirus infection

Senescence induction and sorting of senescent cells

BrdU incorporation assay and Immunofluorescence

Immunoblot

TOP1 ICE (In vivo Complex of Enzyme) Assay and slot blot

Quantitative PCR with reverse transcription

Antibody array

*In vivo* mouse model

Immunofluorescence for tissue sections

QUANTIFICATION AND STATISTICAL ANALYSIS

## KEY RESOURCES TABLE

REAGENT or RESOURCE	SOURCE	IDENTIFIER
Antibodies		
Rat monoclonal anti-BrdU (BU1/75 (ICR1))	Novus	Cat# NB500-169
Rabbit polyclonal anti-TOP1	Proteintech	Cat# 20705-1-AP
Mouse monoclonal anti-Topoisomerase I-DNA Covalent Complexes (TOP1cc) (clone 1.1A)	Millipore	Cat# MABE1084
Mouse monoclonal anti-cGAS (D9)	Santa Cruz	Cat# sc-515777
Rabbit monoclonal anti-STING (D2P2F)	Cell Signaling Technology	Cat# 13647 S
Rabbit polyclonal anti-Cyclin A (H432)	Santa Cruz	Cat# sc-751
Mouse monoclonal anti- $\beta$ -actin	Sigma	Cat# A2228
650 <sup>TM</sup> anti-mouse/human CD11b	Biologend	Cat# 101259
APC/Cyanine7 anti-mouse CD11c	Biologend	Cat# 117324
APC anti-mouse CD4	Biologend	Cat# 100516
PE anti-mouse CD8a	Biologend	Cat# 100708
PE/Cy5 anti-mouse CD69	Biologend	Cat# 104510
Anti-PD-1 antibody (clone 29F.1A12)	Bio X Cell	Cat# BE0273
Mouse anti-CDKN2A/p16INK4a antibody (DSC50.1)	Abcam	Cat# ab1623
Rabbit anti-gamma H2A.X (phospho S139) antibody [EP854(2)Y]	Abcam	Cat# ab81299

Mouse anti-p21(187)	Santa Cruz	Cat# sc-817
Phospho-NF- $\kappa$ B p65 (Ser536) (93H1) Rabbit monoclonal antibody	Cell Signaling Technology	Cat# 3033
NF- $\kappa$ B p65 (D14E12) XP® Rabbit monoclonal antibody	Cell Signaling Technology	Cat# 8242
Phospho-p38 MAPK (Thr180/Tyr182) Antibody	Cell Signaling Technology	Cat# 9211
p38 $\alpha$ MAPK (L53F8) Mouse monoclonal antibody	Cell Signaling Technology	Cat# 9228
Histone H3 (1B1B2) Mouse monoclonal antibody	Cell Signaling Technology	Cat# 14269
Chemicals, Peptides, and Recombinant Proteins		
Cisplatin	Selleck	Cat# S1166
Irinotecan	Selleck	Cat# S2217
5,6-Dimethylxanthenone-4-acetic Acid (DMXAA)	Sigma	Cat# D5817
SPiDER- $\beta$ Gal	Dojindo Molecular Technologies	Cat# SG02-10
5-Bromo-2'-deoxyuridine (BrdU)	Sigma	Cat# B5002
4' 6-Diamidino-2-phenylindole dihydrochloride (DAPI)	Sigma	Cat# D9542
Paraformaldehyde	Sigma	Cat# 158127
Collagenase	Sigma	Cat# C5138
Hyaluronidase	Sigma	Cat# H3884
DNase 1	Sigma	Cat# D5025
Lipofectamine 2000	Thermo Fisher	Cat# 11668019
Hydrochloric acid	Fisher chemical	Cat# SA55
Experimental Models: Cell Lines		
UPK10 ovarian cancer cells		N/A
ID8 ovarian cancer cells		N/A
Lentivirus vectors		
pCMV-GFP	Addgene	Cat# 11153
pLV-mCherry	Addgene	Cat# 36084
pLKO.1-shTOP1 #1( TRCN0000011883)	Wistar Facility	N/A
pLKO.1-shTOP1 #2 (TRCN0000011886)	Wistar Facility	N/A
pLKO.1-shcGAS #1( TRCN0000416658)	Wistar Facility	N/A
pLKO.1-shcGAS #2 (TRCN0000421958)	Wistar Facility	N/A
Critical Commercial Assays		
ACK Lysis Buffer	Thermo Fisher	Cat# A1049201
Live/Dead Fixable Aqua Dead Cell Stain Kit	Thermo Fisher	Cat# L34965
eBioscience fixation/ permeabilization kit	Thermo Fisher	Cat# 88-8824-00
LookOut Mycoplasma polymerase chain reaction (PCR) detection kit	Sigma	Cat# MP0035
Human Topoisomerase 1 ICE Assay Kit	TopoGEN	Cat# TG1020-1
Mouse Cytokine Array C1 kit	RayBiotech	Cat# AAM-CYT-1-2
SuperSignal West Pico PLUS Chemiluminescent Substrate	Thermo Fisher	Cat# 34580

ViraPower kit	Invitrogen	Cat# A11141
Oligonucleotides		
See Table S1		

## CONTACT FOR REAGENT AND RESOURCE SHARING

Further information and requests for resources and reagents should be directed to and will be fulfilled by the Lead Contact, Dr. Rugang Zhang ([rzhang@wistar.org](mailto:rzhang@wistar.org))

## EXPERIMENTAL MODEL AND SUBJECT DETAILS

### Cell lines

The mouse ovarian cancer cell lines UPK10 and ID8 were cultured in RPMI 1640 supplemented with 10% fetal bovine serum (FBS) and 1% penicillin/streptomycin. These cell lines are authenticated at The Wistar Institute's Genomics Facility using short tandem repeat DNA profiling. Regular mycoplasma testing was performed using the LookOut Mycoplasma polymerase chain reaction (PCR) detection (Sigma, Cat. No: MP0035).

### Mice

The protocols were approved by the Wistar Institutional Animal Care and Use Committee (IACUC). Mice are housed in solid bottom, single use ventilated or static cages. Cage bottoms and bedding are changed every two weeks for ventilated cages, and weekly for static. Lids and feeders are changed every 4 weeks. Animal quarters are serviced by individual animal caretakers who are trained to recognize the symptoms characteristic of sick animals. Each day the caretakers initial a checklist posted in each room indicating that observations were made. Temperature and humidity are monitored and documented. Staff monitors for and documents any animal welfare conditions and removes any dead animals if observed and notifies research staff and facility management. If an animal welfare condition is observed both the veterinarian and animal facility director or supervisor are notified. Animals are treated if there are open veterinary cases including weekends and holidays. 6-8-week old female C57BL/6 mouse from CRL/NCI were used for all *in vivo* experiments.

## METHOD DETAILS

### Lentivirus infection and sorting of GFP or mCherry labelled cells

Lentivirus was produced using the ViraPower kit (Invitrogen) based on manufacturer's instructions in the 293FT human embryonal kidney cell line by Lipofectamine 2000 transfection (Thermo Fisher, Cat. No: 11668019). Lentivirus was harvested and filtered with 0.45  $\mu\text{m}$  filter 48 hrs post transfection. Cells infected with lentiviruses were selected in 1  $\mu\text{g}/\text{ml}$  puromycin 48 hrs post infection. GFP or mCherry labelled cells were sorted using flow cytometry.

### Senescence induction and sorting of senescent cells

UPK10 and ID8 cells were treated with 10  $\mu\text{M}$  Cisplatin, 10  $\mu\text{M}$  Irinotecan, or a combination for three days. The drugs were then released from drug treatment and cultured for three days or extended period as indicated. The senescent cells were labelled with SPiDER- $\beta$  Gal Cellular Senescence Detection Kit (Dojindo, Cat. No: SG02-10) following the manufacture's instruction. Both senescent and non-senescent cells were sorted using flow cytometry.

### **BrdU incorporation assay and Immunofluorescence**

Cells were plated on coverslips and labelled with 10  $\mu\text{g/ml}$  BrdU for 24 hrs. Cells were fixed with 4% paraformaldehyde (PFA) for 15 mins at room temperature followed by permeabilization with 0.2% Triton X-100 in PBS for 5 min. Cells were incubated in 2.5 M hydrochloric acid at 4°C for 24 hrs. After blocking with 1% BSA in PBS, cells were incubated with primary antibody overnight at 4°C and Alexa-Fluor conjugated secondary antibody (Life Technologies) for one hr. Fluorescent images were captured using Leica TCS SP5 II scanning confocal microscope.

### **Immunoblot**

Cells were lysed in 1X sample buffer [2% sodium dodecyl sulphate (SDS), 10% glycerol, 0.01% bromophenol blue, 62.5 mM Tris, pH 6.8, and 0.1 M DTT] and heated to 95 °C for 10 mins. Protein concentrations were determined using the protein assay dye (Bio-Rad, Cat. No: #5000006) and Nanodrop. An equal amount of total protein was resolved using SDS polyacrylamide gel electrophoresis gels and transferred to PVDF membranes at 110 V for 2 hrs at 4 °C. Membranes were blocked with 5% nonfat milk in TBS containing 0.1% Tween 20 (TBS-T) for 1 hr at room temperature. Membranes were incubated overnight at 4 °C in the primary antibodies in 4% BSA/TBS + 0.025% sodium azide. Membranes were then washed four times in TBS-T for 5 min at room temperature, after which they were incubated with Horseradish peroxidase-conjugated secondary antibodies (Cell Signaling Technology) for 1 hr at room temperature. After washing four times in TBS-T for 5 min at room temperature, proteins were visualized on film after incubation with SuperSignal West Pico PLUS Chemiluminescent Substrate (Thermo Fisher Scientific).

### **TOP1 ICE (*In vivo* Complex of Enzyme) Assay and slot blot**

Human Topoisomerase 1 ICE Assay Kit (TopoGEN. Cat. No: TG1020-1) was used to isolate protein-DNA samples which contain TOP1-DNA covalent complex (TOP1cc) for slot blot analysis. The isolation was performed following the manufacturer's guidelines.  $5 \times 10^5$  cells were used for ICE assay and TOP1cc analysis. Briefly, cells were lysed with 300  $\mu\text{L}$  of room temperature buffer A, and then 115  $\mu\text{L}$  buffer B was added to precipitate DNA. After washing with buffer C, DNA was dissolved in buffer D and buffer E. The DNA samples were kept in 37 °C to promote the recovery. Nano-Drop was used to measure the DNA concentration. 5  $\mu\text{g}$  DNA was used for each slot blot analysis. Bio-Dot SF Microfiltration Apparatus (Bio Rad. Cat. No: 1706542) was used for slot blot.

### **Quantification PCR with reverse transcription**

Total RNA was isolated using TRIzol (Invitrogen) according to the manufacturer's instruction. Extracted RNAs were used for reverse-transcriptase PCR (RT-PCR) with High-Capacity cDNA Reverse Transcription Kit (Thermo fisher, Cat. No: 4368814). Quantitative PCR (qPCR) was performed using iTaq™ Universal SYBR® Green Supermix (BIO-RAD, Cat. No: 1725121) and QuantStudio 3 Real-Time PCR System. The oligonucleotides used for qPCR analysis were included in **Supplemental Table 1**.

### **Antibody array**

Mouse Cytokine Array C1 kit (RayBiotech. Cat. No: AAM-CYT-1-2) was used for cytokine analysis following the manufacturer's guidelines. Briefly, cells were washed once and cultured in serum-free medium for 48 hrs. Conditioned medium was filtered (0.2  $\mu\text{m}$ ) and then subjected to cytokine-array analysis. After collection of conditional media, the cell number of each sample was counted. The intensities of array dots were visualized on film after incubation with SuperSignal West Pico PLUS Chemiluminescent Substrate (Thermo Fisher Scientific. Cat. No:

34580). The integrated density was measured using Image J and normalized to the cell number from which the conditioned medium was generated.

### ***In vivo* mouse model and profiling of infiltrated immune cells**

The protocols were approved by the Institutional Animal Care and Use Committee of the Wistar Institute.  $1 \times 10^6$  UPK10 cells were unilaterally injected into the ovarian bursa sac of C57BL/6 mouse (female, 6–8 weeks old, CRL/NCI). The orthotopically transplanted cells were allowed to form tumor for 15 days. Tumor-bearing mice were randomly assigned to different treatment groups. The mice were treated for two weeks. Specifically, the mice were pre-treated by i.p. injection ( $1 \times 10^6$  cells per mouse) with control UPK10 cells (group 3), or senescent UPK10 cells sorted from cisplatin, irinotecan and cisplatin/irinotecan combination treated groups (group 4, 5 and 6), or 10 mg/kg DMXAA (group 8), or DMSO vehicle control (group 7). 24 hrs following the pre-treatment, the mice were treated by i.p. injection with anti-PD-1 antibody (Bio X Cell, Cat. No: BE0273, clone 29F.1A12, 10 mg/kg) or an isotype matched IgG control every 3 days.

After two weeks of treatment, the tumors were collected and digested using mixture of 10mg/mL Collagenase (Sigma, Cat No: C5138), 1 mg/mL Hyaluronidase (Sigma, Cat No: H3884) and 200 mg/mL DNase 1 (Sigma, Cat No: D5025) at 37°C for 1 hr. Single-cell suspensions were prepared, and red blood cells were lysed using ACK Lysis Buffer (Thermo Fisher, Cat No: A1049201). Live/dead cell discrimination was performed using LIVE/DEAD™ Fixable Aqua Dead Cell Stain Kit (Thermo Fisher, Cat No: L34968). Cell surface staining was done for 30 min at 4°C. All data acquisition was done using an LSR II (BD) or FACSCalibur (BD) and analyzed using FlowJo software (TreeStar) or the FlowCore package in the R language and environment for statistical computing. For survival analysis, the Wistar Institute IACUC guideline was followed in determining the time for ending the survival experiments (mice succumbed to the disease or tumor burden exceeds 10% of body weight).

### **Immunofluorescence staining for tumor tissue sections**

Formalin-fixed, paraffin-embedded tumors were sectioned, and slides were deparaffinized and rehydrated. Antigen retrieval was performed by boiling for 40 mins in citrate buffer, pH6.0 (Thermo Fisher). Endogenous peroxidases were quenched with 3% hydrogen peroxide in methanol. Sections were then blocked with 5% BSA/PBS at room temperature for 1 hr. Sections were incubated with primary mouse anti-GFP (Santa Cruz, 1:400 dilution) or rabbit anti-mCherry (Proteintech, 1:200 dilution) antibodies at 4°C overnight. Detection was performed using secondary Alexa Fluor 488-conjugated goat anti-mouse IgG (Thermo Fisher, 1:1000 dilution) and Alexa Fluor 555-conjugated goat anti-rabbit IgG (Thermo Fisher, 1:1000 dilution) at room temperature for 1 hr. The sections were counter stained with DAPI containing Duolink® in Situ mounting medium (Sigma Aldrich) and sealed. Samples were imaged on Leica TCS SP5 II Scanning Confocal Microscope.

### **QUANTIFICATION AND STATISTICAL ANALYSIS**

Results are representative of a minimum of three independent experiments. All statistical analyses were conducted using GraphPad Prism 6 (GraphPad). The Student's t-test was performed to determine *P* values of the raw data unless otherwise stated, where *P* < 0.05 was considered significant. Animal experiments were randomized. There was no exclusion from the experiments.